Research article

Tumor-derived extracellular vesicles regulate tumor-infiltrating regulatory T cells via the inhibitory immunoreceptor CD300a

Yuta Nakazawa[1),4)], Kazumasa Kanemaru[1),3)], Chigusa Nakahashi-Oda[1),3)*], Akira Shibuya[1),2),3),*]

[1)] Department of Immunology, Faculty of Medicine, [2)] Life Science Center for Survival Dynamics, Tsukuba Advanced Research Alliance (TARA), [3)] R＆D Center for Innovative Drug Discovery, [4)] Doctoral Program of Biomedical Sciences, Graduate School of Comprehensive Human Sciences, University of Tsukuba, 1-1-1 Tennodai, Tsukuba, Ibaraki 305-8575, Japan

*Correspondence to Akira Shibuya (ashibuya@md.tsukuba.ac.jp) or Chigusa Nakahashi-Oda (chigusano@md.tsukuba.ac.jp)

Abstract

Although tumor-infiltrating regulatory T (Treg) cells play a pivotal role in tumor immunity, how Treg cell activation are regulated in tumor microenvironments remains unclear. Here, we found that mice deficient in the inhibitory immunoreceptor CD300a on their dendritic cells (DCs) have increased numbers of Treg cells in tumors and greater tumor growth compared with wild-type mice after transplantation of B16 melanoma. Pharmacological impairment of extracellular vesicle (EV) release decreased Treg cell numbers in CD300a-deficient mice. Coculture of DCs with tumor-derived EV (TEV) induced the internalization of CD300a and the incorporation of EVs into endosomes, in which CD300a inhibited TEV-mediated TLR3-TRIF signaling for activation of the IFN-β-Treg cells axis. We also show that higher expression of CD300A was associated with decreased tumor-infiltrating Treg cells and longer survival time in patients with melanoma. Our findings reveal the role of TEV and CD300a on DCs in Treg cell activation in the tumor microenvironment.

Introduction

$CD4^+$ regulatory T (Treg) cells specifically expressing Foxp3 play an essential role for maintaining peripheral tolerance, preventing autoimmunity and limiting chronic inflammatory diseases. Deficiency in Treg cells due to genetic inactivation of *Foxp3* or impaired induction of Treg cells after birth results in lethal auto-inflammatory syndromes (Kim et al., 2007; Ramsdell and Ziegler, 2014). Treg cells are found at various tissues, including tumors, at various frequencies. Because tumor-infiltrating Treg cells suppress the activation of tumor antigen-specific $CD8^+$ T cells, a greater proportion of Treg cells to $CD8^+$ T cells among tumor-infiltrating lymphocytes is associated with poor prognosis in several cancers (Nishikawa and Sakaguchi, 2010). Indeed, Treg cell depletion dramatically reduces tumor burden (Klages et al., 2010). Current clinical trials are evaluating strategies targeting receptors (CD25, CTLA-4, CCR4, OX40 and GITR) preferentially expressed on intratumoral Treg cells (Nishikawa and Sakaguchi, 2010; Shitara and Nishikawa, 2018). The migration of Treg cells and their activation and proliferation are regulated by chemoattractants (Adeegbe and Nishikawa, 2013; Ondondo et al., 2013) and cytokines such as

TGF-β and IL-10 (Hsu et al., 2015; Wan and Flavell, 2007). However, how Treg cell activation and proliferation are regulated in the tumor microenvironments remains unclear.

Extracellular vesicles (EVs) are the particles released from the cell that are delimited by a lipid bilayer containing functional biomolecules (proteins, lipids, mRNAs, microRNAs, and DNA fragments) that can be transferred to other cells (Niel et al., 2018; Witwer and Théry, 2019). More than 4,000 trillion EVs are presumed to be in the blood of cancer patients (Melo et al., 2015) and EVs released from tumor cells (tumor-derived EVs;TEVs) are emerging as critical messengers in tumor progression and metastasis (Couto et al., 2018; Grange et al., 2011; Melo et al., 2015; Skog et al., 2008). In tumor immunity, the deleterious role of TEV has been reported that, Fas ligand and PD-L1, the immunomodulatory molecules, on the surface of TEV induce apoptosis or suppression of activated T cells (Andreola et al., 2002; Chen et al., 2018) and TGF-β1 in TEV induces Treg cells (Clayton et al., 2007). Furthermore, macrophages that capture microRNA within EVs are altered to M2 macrophages and promote the malignant behavior of cancers (Wang et al., 2018; Ying

et al., 2016). However, how exosomes regulate immune responses against tumors is not yet fully understood.

The mouse CD300 family molecules, which are encoded by 9 genes on chromosome 11, are expressed on myeloid cells including macrophages, dendritic cells, mast cells and granulocytes and either activate or inhibit innate immune responses (Borrego, 2013; Voss et al., 2015). On the other hand, the human CD300 family consists of 7 molecules encoded by genes located on chromosome 17 in a region syntenic to mouse chromosome 11 (Clark et al., 2001). CD300a, one of the CD300 molecules in mouse, contains an immunoreceptor tyrosine-based inhibitory motif in its cytoplasmic portion. It mediates an inhibitory signal via SHP-1 and SHP-2 by binding to phosphatidylserine, which is exposed on the outer leaflet of the plasma membrane on apoptotic cells and activated mast cells under degranulation (Nakahashi-Oda et al., 2012; Wang et al., 2019; Yotsumoto et al., 2003). Upon binding to phosphatidylserine, CD300a inhibits TLR4-mediated signaling in mast cells and DCs, which results in the suppression of cytokine and chemokine production and modulation of inflammatory immune responses (Nakahashi-Oda et al., 2016, 2012b).

Here, we investigated the role of CD300a in tumor development and demonstrate that CD300a inhibits TEV-mediated interferon-β (IFN-β) production by DCs and suppresses the activation of tumor-infiltrating Treg cells and tumor development.

Results

CD300a on DCs enhances anti-tumor immunity.

To address whether CD300a is involved in tumor immunity, wild-type and CD300a-deficient (*Cd300a*$^{-/-}$) mice were transplanted intradermally with B16 melanoma cells. The *Cd300a*$^{-/-}$ mice showed larger tumor volume and shorter survival than did wild-type mice (Fig. 1**A** and **B**), indicating that CD300a suppresses the development of melanoma. In contrast, Rag-deficient (*Rag1*$^{-/-}$) and *Rag1*$^{-/-}$*Cd300a*$^{-/-}$ mice showed comparable levels of tumor development and survival after injection of B16 melanoma cells (Fig. 1**C** and **D**). These results indicate that the suppressive effect of CD300a on melanoma development is dependent on the adaptive immune response. However, we also observed that CD300a was not expressed on tumor-infiltrating lymphocytes but was broadly expressed on myeloid cells, including populations of Ly6G^{+} neutrophils, CD11c$^{+\sim high}$ DCs, and CD11c^{low}CD11b^{+} macrophages (Fig. S1**A**-**C**). These results suggest that CD300a expressed on myeloid cells suppresses melanoma development via adaptive immune responses. To identify the CD300a-expressing myeloid cell population that is involved in melanoma suppression, we used *Cd300a*$^{fl/fl}$ *Itgax*-Cre and *Cd300a*$^{fl/fl}$

Lys2-Cre mice. *Cd300a*$^{fl/fl}$ *Itgax*-Cre mice expressed CD300a on Ly6G^{+} cells and CD11c^{-} cells, but not on CD11c$^{+\sim high}$ cells (Fig. S1**A**). In contrast, *Cd300a*$^{fl/fl}$ *Lys2*-Cre mice express CD300a on CD11c$^{+\sim high}$ cells and the subpopulation of CD11c^{low} cells, but not on Ly6G^{+} cells (Fig. S1**A**). Although tumor growth was comparable between *Cd300a*$^{fl/fl}$*Lys2*-Cre and *Cd300a*$^{fl/fl}$ mice, *Cd300a*$^{fl/fl}$*Itgax*-Cre mice showed greater tumor volume than did *Cd300a*$^{fl/fl}$ mice (Fig. 1**E**). These data implicated CD300a on DCs, rather than on neutrophils or macrophages, in inducing the adaptive immune response to inhibit tumor development.

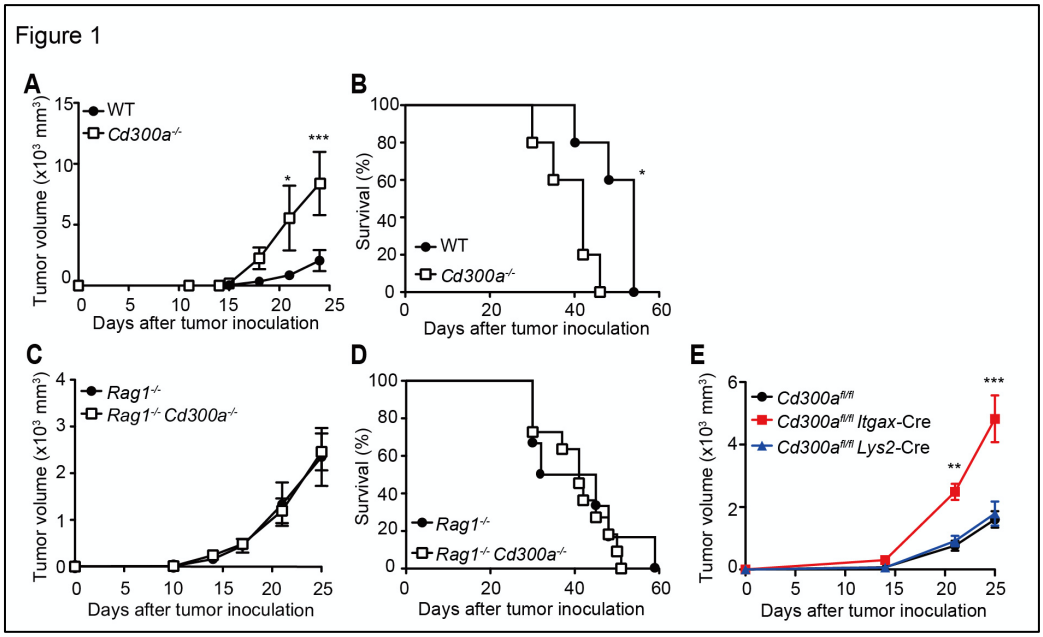

Figure 1. CD300a suppresses tumor growth.
(**A-E**) Tumor growth and survival curves of wild-type (WT, n = 5 in **A** and **B**), *Cd300a*$^{-/-}$ (n = 5 in **A** and **B**), *Rag1*$^{-/-}$ (n = 11 in **C** and n = 6 in **D**), *Rag1*$^{-/-}$ *Cd300a*$^{-/-}$ (n = 11 in **C** and n = 6 in **D**), *Cd300a*$^{fl/fl}$ (n = 7), *Cd300a*$^{fl/fl}$ *Itgax*-Cre (n = 13), and *Cd300a*$^{fl/fl}$ *Lys2*-Cre mice (n = 15) that were inoculated with 1×10^5 B16 melanoma cells on day 0. Data are given as means ± SEMs. **P*<0.05, ***P*<0.01 and ****P*<0.001. *P* values were obtained by using a two-way ANOVA followed by Bonferroni's post-test (**A** and **C**) and the log-rank test (**B** and **D**). Data were pooled from two (**A, B** and **C**) or three (**D** and **E**) independent experiments.

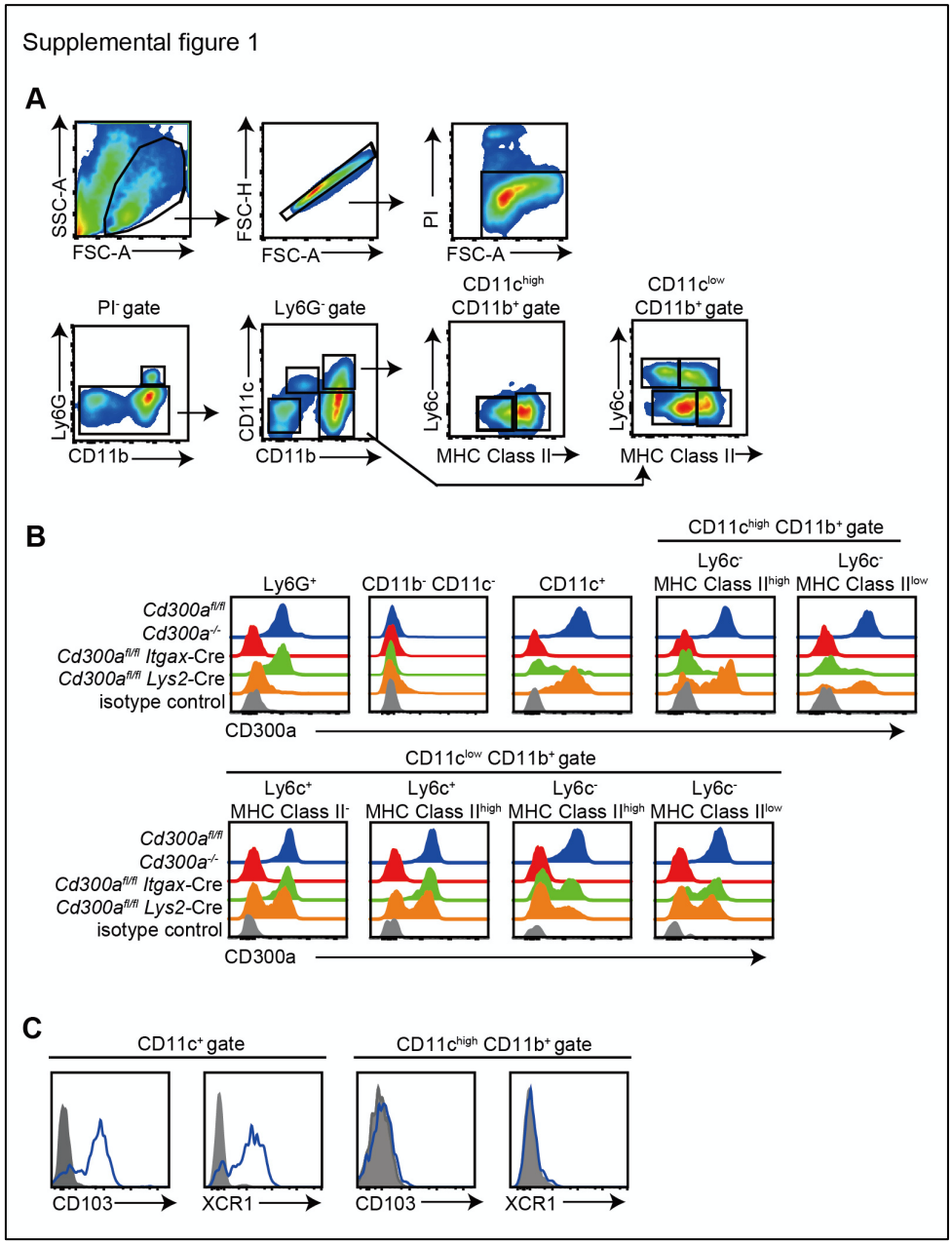

Supplemental figure 1. Expression of CD300a on myeloid cell lineages in tumor infiltrating cells in B16 melanoma.

(**A-C**) Cells isolated from B16 melanoma tissues of *Cd300a*$^{fl/fl}$, *Cd300a*$^{-/-}$, *Cd300a*$^{fl/fl}$ *Itgax*-Cre and *Cd300a*$^{fl/fl}$ *Lys2*-Cre mice prepared 14 days after inoculation were stained with propidium iodide (PI), biotin-conjugated anti-CD300a, APC-Cy7-conjugated CD11b, PE-conjugated Ly6G, FITC-conjugated CD11c, PE-Cy7-conjugated MHC class II, and Alexa-700-conjugated Ly6c antibodies, followed by SA-conjugated APC and analyzed by flow cytometry. (**A**) The populations of Ly6G^{+}, CD11c^{+}, CD11c^{high}CD11b^{+}Ly6C^{-}MHC-II^{high}, CD11c^{high}CD11b^{+}Ly6C^{-}MHC-II^{low}, CD11c^{low}CD11b^{+}Ly6C^{+}MHC-II^{-}, CD11c^{low}CD11b^{+}Ly6C^{+}MHC-II^{high}, CD11c^{-}CD11b^{+}Ly6C^{+}MHC-II^{high}, and CD11c^{-}CD11b^{+}Ly6C^{+}MHC-II^{low} were gated on flow cytometry. (**B**) CD300a expression in each subpopulation is shown. **(C)** CD103 and XCR1 expression on both CD11c^{+} and CD11b^{+}CD11c^{+} cells were analyzed by using specific mAbs. Data are representative of two independent experiments with similar results. Data are representative of three mice.

CD300a regulates tumor-infiltrating Treg cells.

Previous reports have demonstrated that the number of Treg cells in melanoma is correlated with accelerated tumor growth (Mougiakakos et al., 2010). In contrast, depletion of Treg cells leads to less melanoma growth. To elucidate how CD300a on DCs enhances the adaptive immune response against tumor development, we analyzed the population of tumor-infiltrating Treg cells by use of flow cytometry and immunohistochemistry. The Treg cell population was larger in the tumor, but not the draining lymph nodes, of *Cd300a*$^{-/-}$ mice compared with that of wild-type mice (Fig. 2**A** and **B**), whereas the tumor-infiltrating CD8^{+} T cells in *Cd300a*$^{-/-}$ mice produced significantly less IFN-γ than did those in wild-type mice (Fig. 2**C**). Furthermore, PD-1 expression on tumor-infiltrating CD8^{+} T cells in *Cd300a*$^{-/-}$ mice was significantly upregulated compared to that in WT (Fig. 2**D**), suggesting that tumor-infiltrating CD8^{+} T cells in *Cd300a*$^{-/-}$ mice display more exhausted state as previously described(Sawant et al., 2019). To determine whether Treg cells were indeed involved in the exacerbated tumor growth of *Cd300a*$^{-/-}$ mice, we depleted Treg cells by using an anti-CD25 monoclonal antibody (mAb) (Onizuka et al., 1999) (Fig. S2**A**). After Treg cell

depletion, the tumor volume of the *Cd300a*$^{-/-}$ mice decreased to a level comparable to that seen in wild-type mice (Fig. 2**E**). Likewise, the tumor volume decreased in *Cd300a*$^{fl/fl}$*Itgax*-Cre mice to a comparable level to that in *Cd300a*$^{fl/fl}$ mice after depletion of Treg cells (Fig. 2**F**). These results suggest that CD300a on DCs regulates the number of tumor-infiltrating Treg cells, which plays a part in the suppression of tumor development.

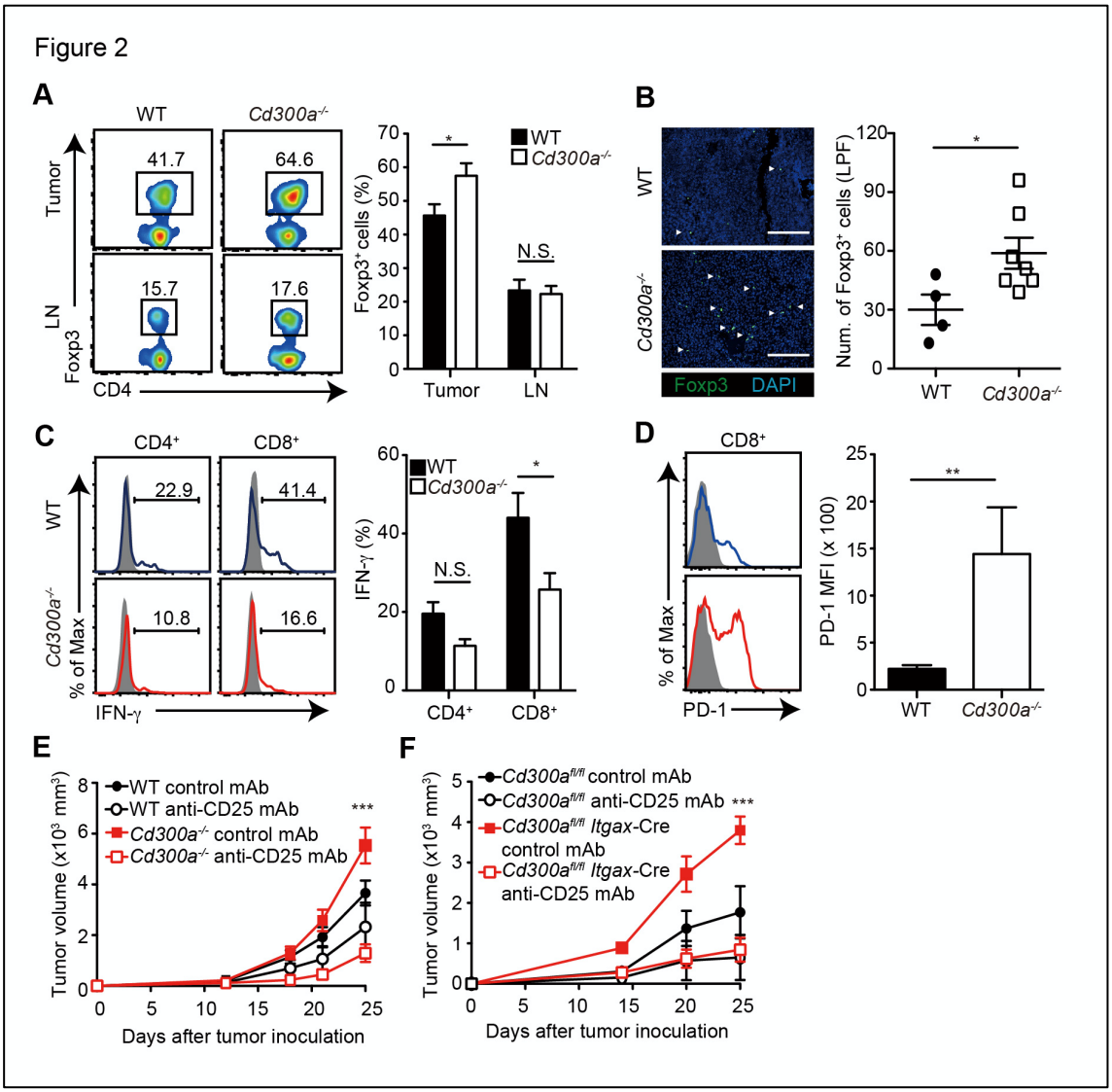

Figure 2. Tumor-infiltrating Treg cells are regulated by CD300a.
Tumor tissues were harvested 3 weeks after B16 melanoma inoculation. (**A**) Representative flow cytometry plots of Treg cells in the tumor and draining lymph node (LN) (left). Numbers adjacent to outlined areas indicate the percentage of Foxp3$^+$ (Treg) CD4$^+$ cells. The frequencies of Foxp3$^+$ cells among CD4$^+$ T cells in both wild-type (WT, n = 7) and *Cd300a*$^{-/-}$ mice (n = 8) are shown (right). (**B**) Fluorescence microscopy of tumor sections from Foxp3-eGFP WT (n = 4) and *Cd300a*$^{-/-}$ (n = 7) mice, stained with an anti-GFP monoclonal antibody (green) and the DNA-binding dye DAPI (left). The number of Foxp3$^+$ cells was quantified from 4 high-power fields (LPF) (right). White arrow shows Foxp3-positive cells. Scale bar, 200 μm. (**C**) Representative histogram of IFN-γ production from tumor-infiltrating T cells after PMA and ionomycin stimulation (left). The proportion of IFN-γ$^+$ cells is shown (right). (n = 6 in each group) (**D**) Representative histogram of PD-1 expression from tumor-infiltrating CD8$^+$ T cells 3 weeks after tumor inoculation (left). The MFI of PD-1 is shown (right). (n = 4 in WT, n = 6 in *Cd300a*$^{-/-}$ mice) (**E** and **F**) Tumor growth curve of WT mice (control mAb, n = 7; anti-CD25 mAb, n = 5) and *Cd300a*$^{-/-}$ (control mAb, n = 8; anti-CD25 mAb, n = 6) or *Cd300a*$^{fl/fl}$ (control mAb, n = 4; anti-CD25 mAb, n = 3) and *Cd300a*$^{fl/fl}$ *Itgax*-Cre (control mAb, n = 3; anti-CD25 mAb, n = 5) mice that were treated with a mAb to CD25 or a control antibody 3 times (Days -6, -3, and 0) and then inoculated with B16 melanoma cells. Data are given as means ± SEMs. N.S.; not significant. **P*<0.05, ***P*<0.01 and ****P*<0.001. *P* values were obtained by using a two-way ANOVA followed by Bonferroni's post-test (**A**, **C**, **D**) and the student's *t*-test (**B** and **D**). Data were pooled from two (**B**, **D** and **E**) or three (**A**, **C** and **D**) independent experiments.

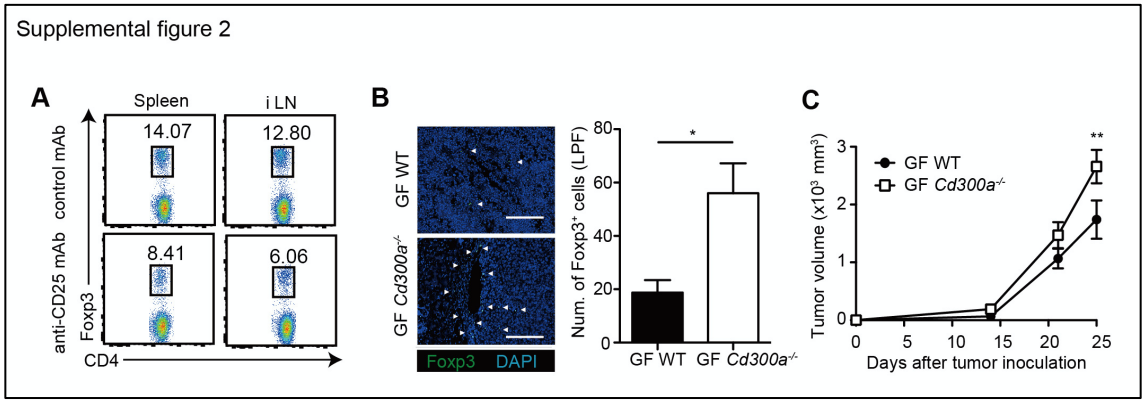

Supplemental figure 2. Tumor growth in *Cd300a*$^{-/-}$ mice is independent of the microbiota
(**A**) Flow cytometric analysis of Foxp3$^+$ cells in the spleen and inguinal lymph node (iLN) of mice injected with isotype mAb and 300 μg of anti-CD25 mAb on Days -6 and -3 prior to analysis. (**B**) Representative fluorescence micrographs of tumor sections from germ-free (GF) wild-type (WT) and *Cd300a*$^{-/-}$ mice and stained with an anti-Foxp3 monoclonal antibody (green) and the DNA-binding dye DAPI (left). The number of Foxp3$^+$ cells was quantified from 4 high-power fields (LPF) (right). White arrows show Foxp3-positive cells. Scale bar, 200 μm. (**C**) Comparison of tumor growth of B16 melanoma between GF WT (n = 5) and *Cd300a*$^{-/-}$ mice (n = 6). Data are given as means ± SEMs. **P*<0.05 and ***P*<0.01. *P* values were obtained by using the student's test (**B**) and a two-way ANOVA followed by Bonferroni's post-test (**C**). Data were pooled from two independent experiments (**A**-**C**).

Tumor-derived exosomes augment IFN-β production and consequent tumor development.

We previously reported that a microbiota-mediated signal induces increased IFN-β production by DCs and increased numbers of Treg cells in the barrier tissues such as the intestine, skin, and airway of *Cd300a*$^{-/-}$ mice relative to those of wild-type mice (Nakahashi-Oda et al., 2016). In the current study, we found that the expression of *Ifnb* was also higher in DCs in the tumor tissues of *Cd300a*$^{-/-}$ mice than in those of wild-type mice (Fig. 3**A**). To examine whether the microbiota is also involved in Treg cell levels in the tumor and tumor growth, we used wild-type and *Cd300a*$^{-/-}$ mice raised under the germ-free (GF) conditions. In contrast to the barrier tissues, *Cd300a*$^{-/-}$ mice still showed larger numbers of Treg cells and a larger tumor volume than did wild-type mice raised under GF conditions (Fig. S2**B** and **C**). These results suggest that, unlike in the barrier tissues, the microbiota-mediated signal was dispensable for the increased numbers of Treg cells in the tumor and for the enhanced tumor growth in *Cd300a*$^{-/-}$ mice.

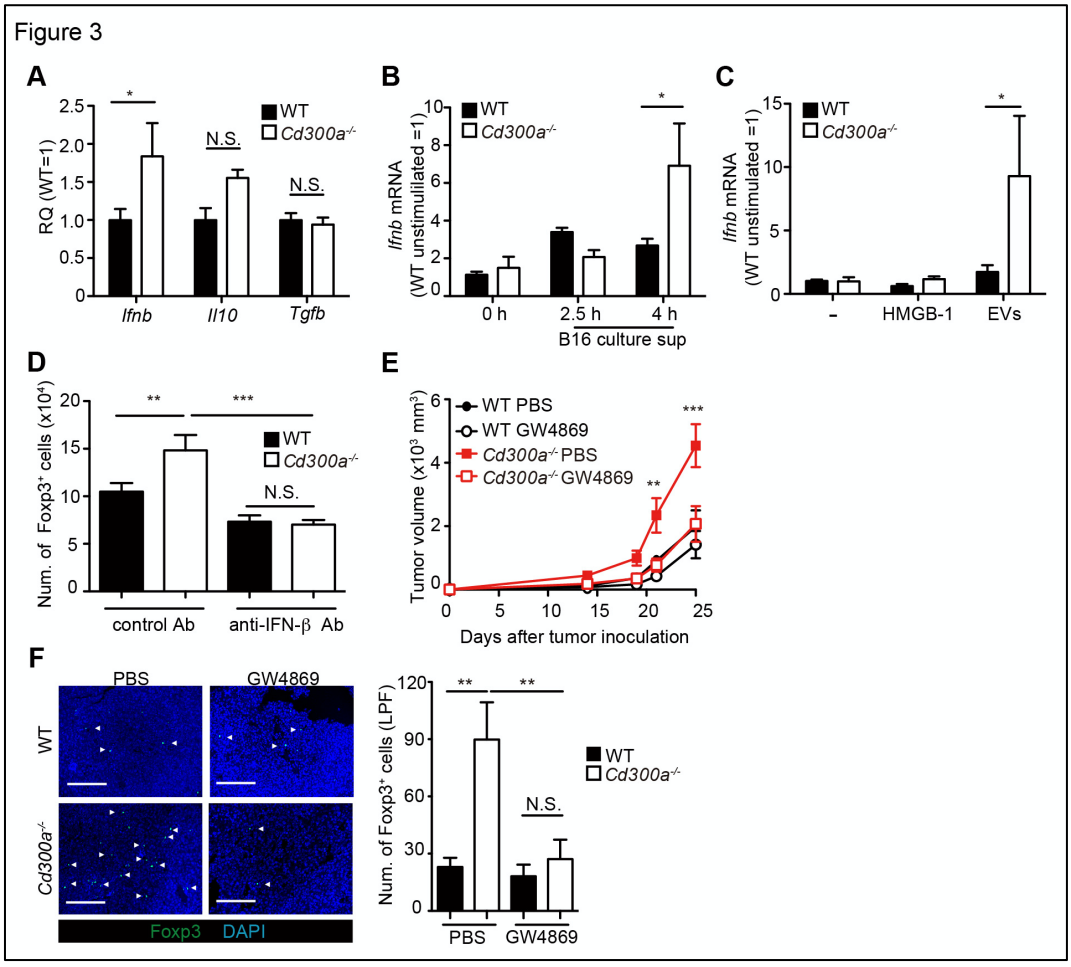

Figure 3. Tumor-derived EVs facilitate IFN-β production from dendritic cells and promote tumor-infiltrating Treg cell accumulation.

(**A**) Quantitative RT-PCR analysis of mRNA from CD11c^{+} cells sorted from B16 melanoma in wild-type (WT, n = 6) and *Cd300a*$^{-/-}$ (n = 6) mice 2 weeks after tumor inoculation. Results are presented relative to those of the control gene encoding β-actin. (**B**) Quantitative RT-PCR analysis of *Ifnb* in WT- and *Cd300a*$^{-/-}$-derived BMDCs that received no treatment (0 h, n = 7) or B16 culture supernatants (2.5 h, n = 5; 4.0 h, n = 7). (**C**) Quantitative RT-PCR analysis of *Ifnb* in WT- and *Cd300a*$^{-/-}$ -derived BMDCs that received no treatment (-) (n = 6 in each group) and were treated with HMGB-1 (n = 3 in each group) or B16-derived extracellular vesicles (EVs, n = 5 in each group). (**D**) The number of induced Foxp3-eGFP^{+} cells (iTreg) generated from naïve T cells by using anti-CD3, anti-CD28, IL-2 and TGF-β. These iTreg cells were cocultured with EV-stimulated BMDCs in the presence of IL-2 and TGF-β for 5 days with a control mAb (n = 7) or an anti-IFN-β mAb (n = 5). (**E**) Tumor growth curves of WT (PBS, n = 6; GW4869, n = 9) and *Cd300a*$^{-/-}$ mice (PBS, n = 7; GW4869, n = 9) that were treated with GW4869 or PBS 3 times (Days 14, 18, and 21). (**F**) Representative fluorescence micrographs of tumor sections from Foxp3-eGFP WT (PBS, n = 4; GW4869, n = 6) and Foxp3-eGFP *Cd300a*$^{-/-}$ mice (PBS, n = 5; GW4869, n = 6) in the absence or presence of GW4869, and stained with an anti-GFP monoclonal antibody (green) and the DNA-binding dye DAPI (left). The number of Foxp3^{+} cells was quantified from 4 high-power fields (LPF) (right). White arrow shows Foxp3-positive cells. Scale bar, 200 μm. Data are given as means ± SEMs. RQ; relative quantification. N.S.; not significant. **P*<0.05, ***P*<0.01 and ****P*<0.001. *P* values were obtained by using a one-way ANOVA (**D** and **F**) and a two-way ANOVA followed by Bonferroni's post-test (**A**, **B**, **C**, and **E**). Data were pooled from two (**D** and **F**) or three (**A**, **B**, **C** and **E**) independent experiments.

Solid tumors lapse into necrosis in the core region under conditions of hypoxia and low pH, resulting in the secretion of several immune stimulators, such as danger-associated molecular patterns (DAMPs), DNA, RNA (Patidar et al., 2018) and EVs (Couto et al., 2018). We examined whether the culture supernatant of B16 melanoma cells containing tumor-derived immune mediators had any effect on *Ifnb* expression by using cultured bone marrow-derived dendritic cells (BMDCs). Four hours after incubation in the presence of the culture supernatant, *Cd300a*$^{-/-}$ BMDCs expressed higher levels of *Ifnb* than did wild-type BMDCs (Fig. 3**B**), suggesting that CD300a suppressed the *Ifnb* expression induced by a tumor-derived immune mediator in the culture supernatant. Since EVs are the particles released from the cells that are delimited by a lipid bilayer that contains phosphatidylserine (Lima et al., 2009), the ligand for CD300a (Nakahashi-Oda et al., 2012a), and containing functional biomolecules (Niel et al., 2018), we focused on EVs. We purified EVs from the culture supernatants of B16 melanoma cells by centrifugation and phosphatidylserine receptor-conjugated beads (Fig. S3**A**), which indeed expressed phosphatidylserine on the surface and bound to a chimeric fusion protein of the extracellular portion of

166 CD300a with human IgG1 (Fig. S3**B**). Stimulation with the purified EVs induced higher

167 *Ifnb* expression in *Cd300a*$^{-/-}$ BMDCs than in wild-type BMDCs (Fig. 3**C**). In contrast,

168 neither wild-type nor *Cd300a*$^{-/-}$ BMDCs expressed IFN-β after stimulation with a

169 damage associated molecular patterns (DAMPs) high mobility group box-1 protein

170 (HMGB-1) (Fig. 3**C**), which can be released by damaged tumors. These results suggest

171 that CD300a suppresses TEV-induced IFN-β production in DCs.

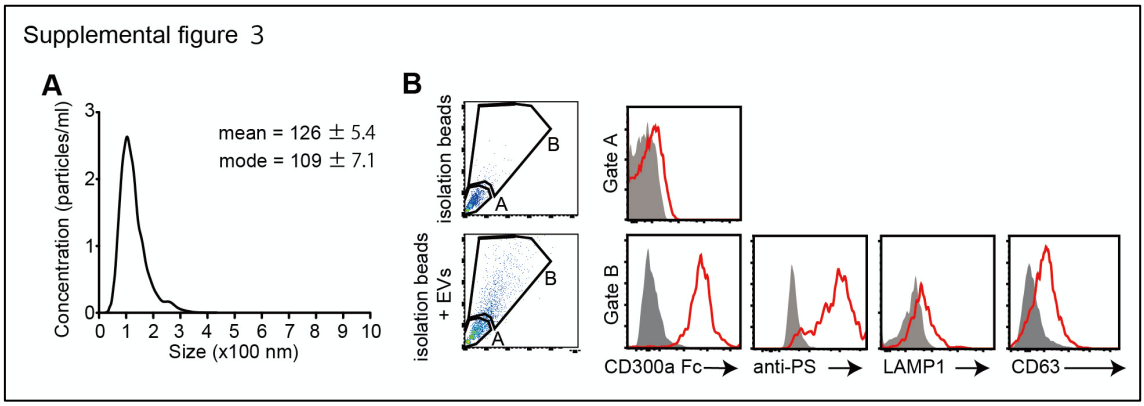

Supplemental figure 3. CD300a binds to B16-derived EVs.
(**A**) The size distribution of isolated B16-derived EVs was analyzed by NTA using NanoSight LM10. (**B**) Flow cytometric data of EVs isolated from B16 melanoma supernatants. Bead-conjugated EVs were analyzed by flow cytometry and characterized by the indicated antibody in the presence of 2 mM $CaCl_2$.

172 To clarify whether IFN-β enhances Treg cell proliferation, we cocultured

173 TEV-stimulated wild-type or *Cd300a*$^{-/-}$ BMDCs with Treg cells that were generated

174 from naïve CD4$^+$ T cells from Foxp3-eGFP$^+$ mice in the presence of anti-CD3 and

175 anti-CD28 mAbs, IL-2, and TGF-β. TEV-stimulated *Cd300a*$^{-/-}$ BMDCs increased the

number of Treg cells to a greater extent than did TEV-stimulated wild-type BMDCs (Fig. 3**D**). Addition of a neutralizing anti-IFN-β antibody to the coculture of Treg cells and *Cd300a*$^{-/-}$ BMDCs reduced the Treg cell numbers to a level comparable to that seen in the coculture of Treg cells and wild-type BMDCs (Fig. 3**D**), suggesting that IFN-β augmented Treg cell proliferation or survival. To investigate the effects of TEV on Treg cells, we injected an EV-release inhibitor GW4869 (Ikebuchi et al., 2018) into the tumor region on day 10, 14 and 18 after tumor inoculation. Treatment with GW4869 led to a significant decrease in the number of tumor-infiltrating Treg cells and the tumor volume (Fig. 3**E** and **F**). Taken together, these results indicate that CD300a suppresses EV-mediated IFN-β production, resulting in a decrease in the Treg cell population and the suppression of tumor development.

CD300a inhibits the EV-induced TLR3-TRIF signaling for IFN-β production.

To further analyze how CD300a regulates TEV-mediated IFN-β production in DCs, we cocultured pHrodo- or PKH-labeled exosomes with wild-type or *Cd300a*$^{-/-}$ BMDCs and analyzed the localization of the TEVs in BMDCs by using confocal laser scanning

192 microscopy. We found that the TEVs were incorporated into endosomes, as identified
193 by the expression of endosome antigen (EEA)-1, in both genotypes of DCs (Fig. 4**A**).
194 The number of TEVs in the endosomes was comparable between wild-type and
195 *Cd300a*$^{-/-}$ BMDCs (Fig. 4**B**), suggesting that CD300a did not affect TEV incorporation
196 into the endosomes. Interestingly, we also found that CD300a was internalized from the
197 cell surface into the endosomes, an event that might be mediated by the tyrosine-based
198 sorting motif in the cytoplasmic region of CD300a (Yotsumoto et al., 2003), after
199 coculture of BMDCs with TEVs (Fig. 4**C** and Fig. S4**A**). As a result, the TEVs
200 colocalized with CD300a at the endosomes (Fig. 4**A** and **C**). Given that EVs expose
201 phosphatidylserine on their lipid bilayer, which is a CD300a ligand, these results
202 suggest that CD300a was activated via stimulation with TEVs at the endosomes.

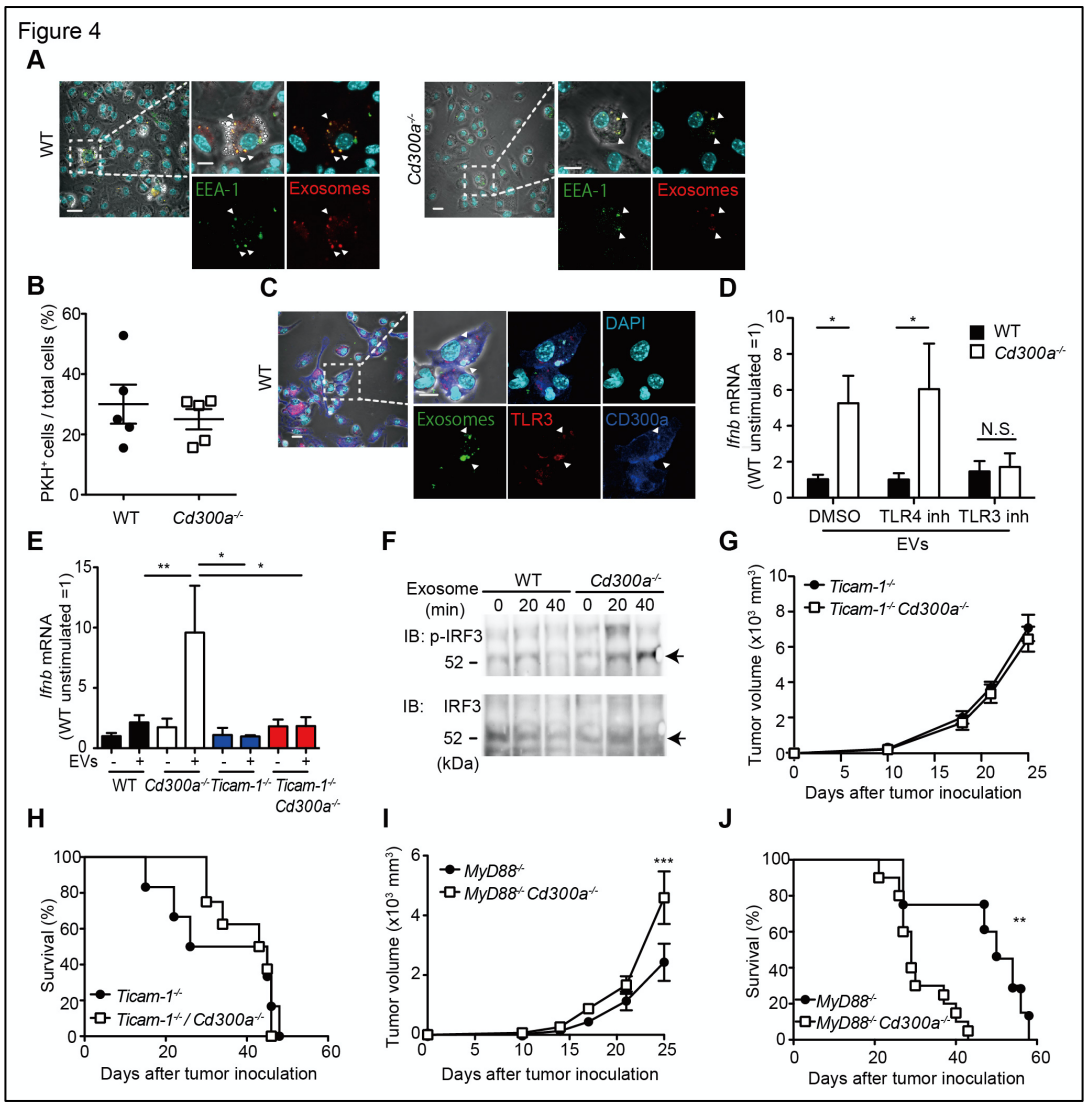

Figure 4. CD300a inhibits TLR3-mediated IFN-β expression upon recognition of tumor-derived EVs.

(**A**) Representative microscopy images of wild-type (WT) and *Cd300a*$^{-/-}$ bone marrow-derived dendritic cells (BMDCs) treated with pHrodo-labeled EVs to assess the localization of EVs (red) and early endosome antigen (EEA)-1 (green). Scale bar, 10 μm. Data are representative of two independent experiments. (**B**) Uptake of PKH-labeled TEVs in WT (n = 5) and *Cd300a*$^{-/-}$ BMDCs (n = 5). (**C**) Representative microscopy images of WT and *Cd300a*$^{-/-}$ BMDCs treated with pHrodo-labeled EVs to assess the localization of exosomes (green), TLR3 (red), and CD300a (blue). Scale bar, 10 μm. Data are representative of two independent experiments. (**D**) Quantitative RT-PCR analysis of *Ifnb* in WT and *Cd300a*$^{-/-}$ BMDCs treated with B16-derived EVs in the presence of DMSO (WT, n = 9; *Cd300a*$^{-/-}$, n = 10), 100 nM TLR4 inhibitor (n=7 in each group), and 50 μM TLR3 inhibitor (n = 6 in each group). (**E**) Quantitative RT-PCR analysis of *Ifnb* in WT, *Cd300a*$^{-/-}$, *ticam-1*$^{-/-}$, and *ticam-1*$^{-/-}$ *Cd300a*$^{-/-}$ mice-derived BMDCs treated with B16-derived EVs (n = 5 in all group). (**F**) Representative immunoassay of WT and *Cd300a*$^{-/-}$ BMDCs left unstimulated (0 min) or stimulated for the indicated times with B16-derived exosomes, followed by immunoblot analysis of phosphorylated (p-) IRF3 or total IRF3. Data are representative of two independent experiments. (**G** and **H**) Comparison of tumor growth and survival curves of B16 melanoma cells between *ticam-1*$^{-/-}$ (n = 6) and *ticam-1*$^{-/-}$ *Cd300a*$^{-/-}$ mice (n = 9) after inoculation of B16 melanoma. (**I** and **J**) Comparison of tumor growth and survival curves of B16 melanoma between *MyD88*$^{-/-}$ (n = 9) and *MyD88*$^{-/-}$ *Cd300a*$^{-/-}$ mice (n = 10) after inoculation of B16 melanoma. Data are given as means ± SEMs. N.S; not significant **P*<0.05, ***P*<0.01 and ****P*<0.001. *P* values were obtained by using the student's *t*-test (**B**), a two-way ANOVA followed by Bonferroni's post-test (**D**, **E**, **G** and **I**) and the log-rank test (**H** and **J**). Data were pooled from two (**B**, **E** and **H**) or three (**D**, **I** and **J**) independent experiments.

EVs also contain nucleic acids, including structured RNA (Liu et al., 2016; Niel et al., 2018). TLR3 at the endosomal membrane can recognize RNA and mediates IFN-β production via the TRIF signaling pathway in DCs (Tatematsu et al., 2013). To examine whether CD300a inhibited TLR3-mediated signaling at the endosomes upon stimulation with TEVs, we cocultured wild-type and *Cd300a*$^{-/-}$ BMDCs with TEVs in the presence of an inhibitor of TLR3 (Cheng et al., 2011). This inhibitor decreased *Ifnb* expression in *Cd300a*$^{-/-}$ BMDCs to a level comparable to that in wild-type BMDCs (Fig. 5**D** and Fig. S4**B**). In contrast, the TLR4 inhibitor TKA-242 did not affect the expression of *Ifnb* in either BMDC genotype (Fig. 4**D** and Fig. S4**B**). These results suggest that CD300a inhibits TLR3-mediated signaling for IFN-β production. Moreover, the expression of *Ifnb* in *ticam-1*$^{-/-}$ *Cd300a*$^{-/-}$ BMDCs was also decreased to the comparable level of that in *ticam-1*$^{-/-}$ BMDCs after coculture with TEVs (Fig. 4**E**). In addition, we found that the phosphorylation level of interferon regulatory factor 3 (IRF3), a downstream molecule of the TRIF signaling pathway, was increased to a greater extent in EV-stimulated *Cd300a*$^{-/-}$ BMDCs than in wild-type BMDCs (Fig. 4**F**). In vivo analyses also showed that, although tumor growth was significantly larger and

220 the survival rate was significantly shorter for B16 melanoma-injected *Myd88*$^{-/-}$ *Cd300a*$^{-/-}$

221 mice compared with B16-injected *Myd88*$^{-/-}$ mice, tumor development and survival did

222 not differ between *ticam-1*$^{-/-}$ *Cd300a*$^{-/-}$ and *ticam-1*$^{-/-}$ mice (Fig. 4**G-J**). Taken together,

223 these data suggest that CD300a inhibits the TLR3-TRIF signaling pathway for IFN-β

224 production at the endosomes in DCs, resulting in the suppression of Treg cell activation

225 and tumor development.

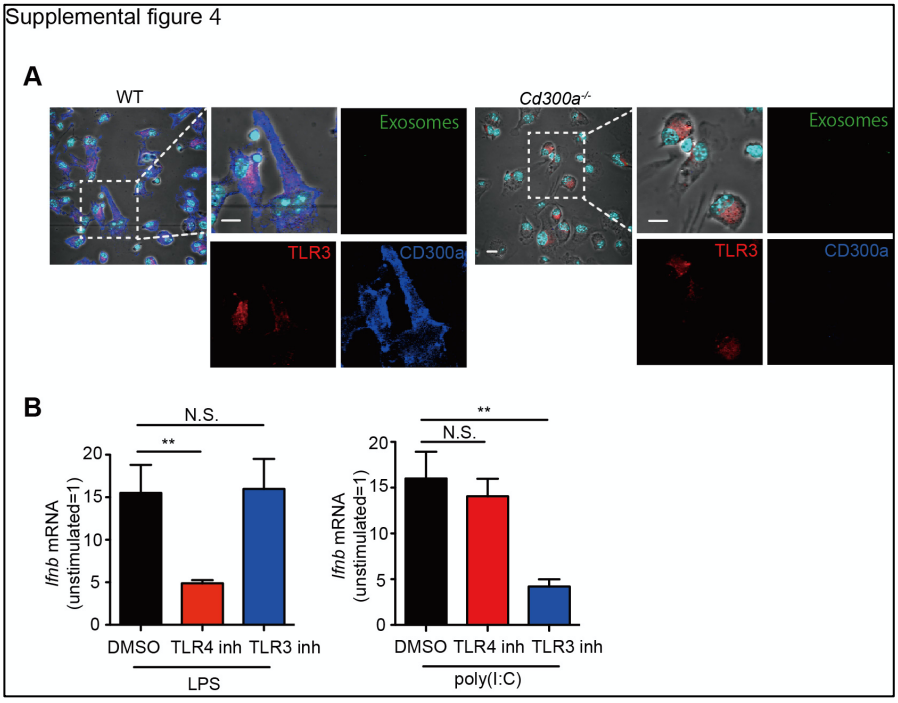

Supplemental figure 4. CD300a is localized on the surface of plasma membrane without stimulation.
(**A**) Representative confocal microscopy images of BMDCs stained with anti-TLR3 and anti-CD300a mAbs. (**B**) Quantitative RT-PCR analysis of *Ifnb* in BMDCs stimulated with LPS or poly(I;C) in the presence of TLR4 or TLR3 inhibitors (LPS and poly(I;C), n = 12 in each group; TLR4 and TLR3 inhibitors, n = 9 in each group). Data are given as means ± SEMs. N.S; not significant. ***P*<0.01. *P* values were obtained by using a one-way ANOVA followed by Bonferroni's post-test (**B**). Data were pooled from two (**A**) three (**B**) independent experiments.

226 ***CD300A* expression associates with survival times in melanoma patients.**

227 To examine the role of CD300A in tumor development in humans, we analyzed the data
228 on the single-cell RNA sequence of human melanoma tissues, which demonstrated that
229 *CD300A* is expressed on populations that express *HLA-DR, ITGAX (CD11c), ITGAM*
230 *(CD11b), CD14*, and *CD163* (Fig. S5), consistent with the results of mouse melanoma.
231 We further analyzed the database of the Cancer Genome Atlas (TCGA) project and
232 found that skin cutaneous melanoma patients (SKCM) expressing low levels of
233 *CD300A* mRNA had shorter survival times than did those expressing higher *CD300A*
234 mRNA levels (Fig. 5**A**). We also found that the expression ratio of *CD300A* to *ITGAX*
235 is negatively correlated with that of *FOXP3* to *CD8A* (Fig. 5**B**). These results suggested
236 that CD300A suppressed Treg cell proliferation and/or activation and tumor
237 development. Moreover, we found that patients with melanoma showed strong positive
238 correlation between *FOXP3* and *IFNB1* expression (Fig. 5**C**). Neutral
239 sphingomyelinase-2 (SMPD3), which is a target of an inhibitor of EV release GW4869,
240 enhances EV release from tumor cells (Kosaka et al., 2013, 2010). TCGA database of
241 SKCM also showed a strong positive correlation between expressions of *SMPD3* and

242 *IFNB1* in melanoma tissues (Fig. 5**D**), suggesting that EVs increased IFN-β expression

243 in human melanoma tissues. These results were consistent with those of mouse models

244 of melanoma development in the current study. Taken together, these results suggested

245 that CD300A might augment tumor immunity via suppression of tumor-infiltrating Treg

246 cells also in humans.

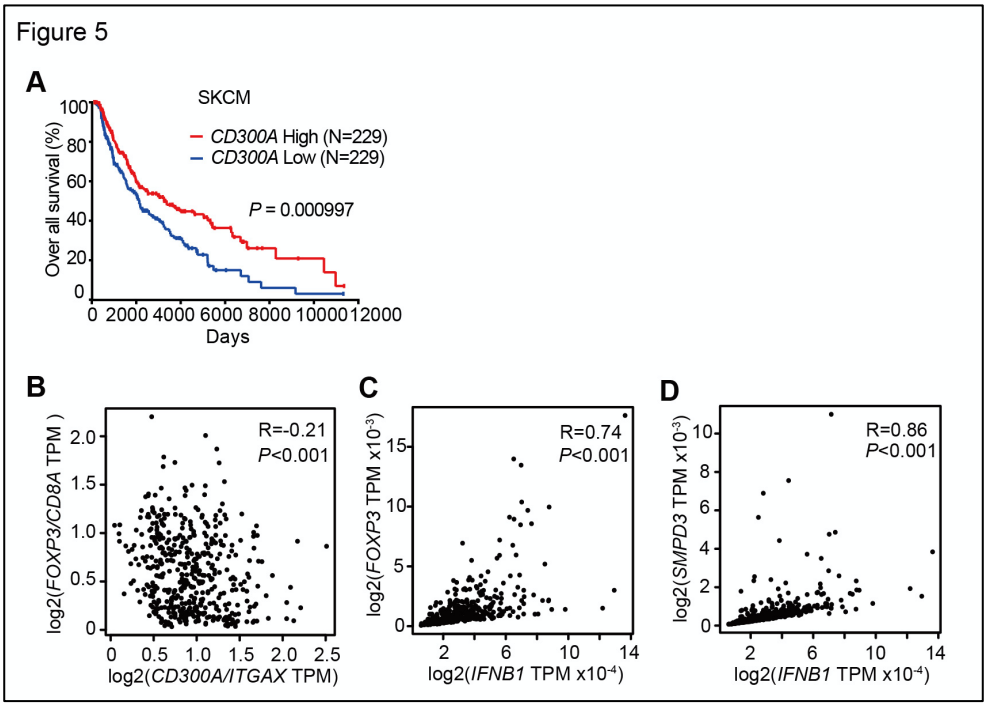

Figure 5. *CD300A* expression associates with survival of human melanoma patients. (**A**) Kaplan plot showing low and high *CD300A* expressions in skin cutaneous melanoma (SKCM) patients obtained by performing a meta-analysis of TCGA database. Median values were used as thresholds. (numbers of both low and high expression patients = 229) (**B-D**) Spearman correlation analysis of TCGA skin cutaneous melanoma database by using GEPIA2. *FOXP3, IFNB1* and *SMPD3* expression were normalized by *GAPDH* expression (**C, D**).

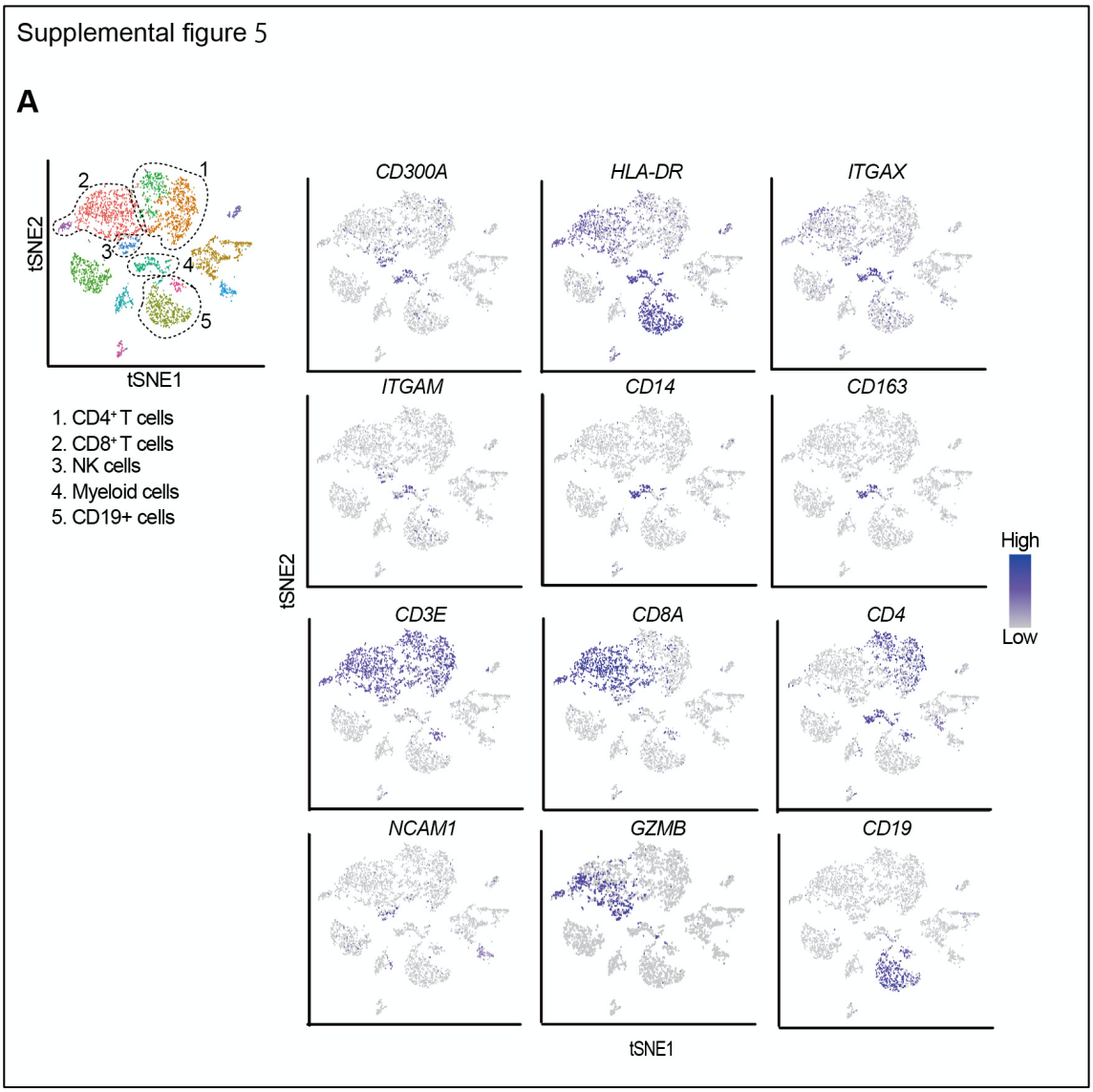

Supplemental figure 5. tSNE plots of the immune cell landscape isolated from melanoma patients.

Indicated gene expressions were reanalyzed by using GSE76056. Cell clusters of $CD4^+$ T cells, $CD8^+$ T cells, NK cells, myeloid cells and $CD19^+$ cells were determined by *CD4/CD3E*, *CD8A/CD3E*, *NCAM1(CD56)/GZMB*, *ITGAM(CD11b)*/*ITGAX(CD11c)*/HLA-DR/CD14/CD163 and *CD19* expression, respectively.

247

Discussion

Although the biological roles of EVs have been reported from various angles, how EVs regulate immune responses is not yet fully understood. In the present study, we showed that TEV stimulated DCs for IFN-β production via TLR3 at the endosomes, resulting in the increased number of tumor-infiltrating Treg cells and thus the exacerbation of tumor development. In contrast, the TEVs also stimulated CD300a and inhibited TEV-mediated TLR3 signaling at the endosome. Thus, TEVs have both positive and negative functions in the regulation of IFN-β production and Treg activation via the axis of EV-derived RNA-TLR3 and EV-derived phosphatidylserine-CD300a, respectively. These results suggest that the Treg cells in tumor microenvironments is regulated by the balance of positive and negative signaling for IFN-β production induced by TEV. Hence, it is an interesting issue to be examined whether the expressions of RNAs are different among TEVs derived from tumors of variable tissue types.

On the other hand, the balance of TLR3 and CD300a expressions in DCs may also be important for Treg activation and tumor development. Indeed, we showed that higher expression of CD300A was associated with lower expression of Foxp3 and

longer survival times of melanoma patients. While previous reports demonstrated that TEVs promoted Treg cell expansion through DCs-independent manner *in vitro* (Muller et al., 2017; Szajnik et al., 2010; Wieckowski et al., 2009), the current study first demonstrated that TEVs regulate Treg cell activation and tumor development *in vivo* by DCs in the tumor microenvironment. Meanwhile, Tumor-infiltrating DCs are heterogenous, and can be divided into at least two subsets. The conventional type-1 DC (cDC1) expresses the chemokine receptor XCR1 and CD103 and lower amount of CD11b that has the high ability to migrate from tumors to lymph nodes and presents a tumor antigen to $CD8^+$ T cells (Bedoui et al., 2009). In contrast, the conventional type-2 DC (cDC2) are commonly distinguished from cDC1 by their preferential expression of higher amount of CD11b. cDC2 are predominantly involved in antigen presentation by MHC class II to $CD4^+$ T cells (Gao et al., 2013). Given that cDC2 is involved in $CD4^+$ T cell differentiation and activation, CD300a on cDC2, rather than cDC1, may regulate Treg cells activation by inhibiting the TLR3-IFN-β pathway in tumor microenvironment.

Type I IFNs are key players in antiviral and anticancer immune response by

upregulating both cross-presentation of antigens by $CD8a^+$ DCs and cytotoxic activity of $CD8^+$ T cells and NK cells (Zitvogel et al., 2015). However, the current clinical use of IFN-β for cancers showed limited efficiency (Medrano et al., 2017; Minn, 2015). This might be, in part, because type I IFN also has immunosuppressive function. IFNs are most potent cytokines to induce PD-L1 on Treg cells (Morimoto et al., 2018; Xiao et al., 2018), which contributes to sustain Foxp3 expression and promotes the function of Treg cells (Francisco et al., 2009). In addition, IFN-α/β receptor signaling promotes Treg cell development (Metidji et al., 2015). We previously reported that gut commensals stimulated $CX3CR1^+CD103^-$ $CD11b^+$ DCs to produce IFN-β, which augmented the proliferation of Treg cells in the intestine (Nakahashi-Oda et al., 2016). In contrast, published reports demonstrated that, in viral infection and tumor microenvironment, type I IFNs directly inhibits the proliferation and activation of Treg cells (Gangaplara et al., 2018; Srivastava et al., 2014). Further investigations are required to clarify the molecular mechanism underlying this controversial issue.

We have previously reported that CD300a inhibited the CD14-mediated TLR4 internalization in $CD11b^+$ DCs induced by gut microbiota (Nakahashi-Oda et al.,

296 2016). In the present study, we demonstrated that CD300a inhibited the
297 TLR3-mediated TRIF signaling at the endosome. These results indicate that CD300a
298 inhibits different TLRs-mediated signaling induced by different ligand providers. TLR3
299 activates PI3 kinase and the downstream kinase, Akt, leading to full phosphorylation
300 and activation of IRF3(Sarkar et al., 2004). Indeed, we showed that IRF3
301 phosphorylation was increased in *Cd300a*$^{-/-}$ DCs compared with wild-type DCs after
302 stimulation with TEV. Recent studies have revealed that TLR3 on alveolar epithelial
303 cells recognized RNAs in TEV and promoted lung metastasis (Liu et al., 2016).
304 Therefore, the role of RNAs in TEV is dependent on target cells. Our findings thus
305 highlighted the role of TEV and CD300a on DCs in the regulation of tumor-infiltrating
306 Treg cells and tumor immunity.
307

Materials & Methods

Mice

All gene-edited mice in the C57BL/6J background were previously described(Nakahashi-Oda et al., 2016). C57BL6J mice and GF mice were purchased from Clea Japan and Sankyo Laboratory, respectively. GF mice were bred and maintained in vinyl isolators to maintain GF conditions. Mice were used for the experiments at 8 to 12 weeks of age. All experiments were performed in accordance with the guidance of the animal ethics committee of the University of Tsukuba Animal Research Center.

Antibodies, flow cytometry, and reagents

The isotype-matched control antibodies rat IgG2a (553928), rat IgG1 (553921), and mouse IgG1 (553445), as well as mAbs to CD4 (RM4-5), CD8 (53-6.7), CD11b (M1/70), CD11c (HL3), I-A^b (M5/114.15.2), Ly6C (AL-21), Ly6G (1A8), CD62L (MEL-14), CD44 (IM7), and IFN-γ (XMG1.2) were purchased from BD Bioscience. Mabs to CD63 (NVG-2), CD103 (2E7), XCR1 (ZET) were purchased from Biolegend.

Anti-IFN-β (7F-D3) was from Yamasa; control rat IgG (6130-01) was purchased from Southern Biotechnology. Anti-PS antibody (1H6) was purchased from Merck Millipore. The CD300a-specific mAb (EX42) was generated in our laboratory. Anti-CD25 (PC61) was a gift from E. Nakayama (Okayama University). Cells were treated for 10 min with anti-CD16/32 mAb (2.4G2; TOMBO Bioscience) to prevent binding to FcγR prior to incubation with the indicated combination of antibodies. All samples were evaluated by using a Fortessa flow cytometer (Becton Dickinson) and analyzed by using FlowJo software (Tree Star).

Tumor cell maintenance and injection

The B16 mouse melanoma cells were obtained from RIKEN Cell Bank (Tsukuba, Japan). Cells were maintained in RPMI-1640 (Sigma) supplemented with 5% (v/v) fetal bovine serum (FBS) (Thermo Fisher). To inoculate the tumor cells into mice, cells were harvested by trypsinization, washed with sterile PBS, and injected intradermally (2×10^5 cells/50 μl sterile PBS/mouse) on the flank of each mouse. Tumor growth was measured every 3 or 4 days by using a caliper.

340

341 **Cell preparations**

342 For tumor-infiltrating Treg cell preparation, tumor tissues were harvested 3 weeks after
343 tumor inoculation. Tumor tissues were cut into small pieces, incubated in 5% FBS
344 RPMI-1640 in the presence of an enzyme mixture (Miltenyi Biotec) at 37℃ for 45 min,
345 and digested by using a gentleMACS Dissociator and tumor dissociation kit (Miltenyi
346 Biotec), according to the manufacturer's instructions. Cells were filtered through 70-μm
347 nylon mesh and subsequently centrifuged using different concentrations of Percoll
348 (Sigma-Aldrich) to exclude tissue debris and were washed with staining medium.
349 BMDCs were generated as described previously (Nakahashi-Oda et al., 2016).
350 Briefly, bone marrow cells were cultured in a 10-cm culture dish in complete RPMI
351 1640 containing 10% FBS in the presence of 10 ng/ml GM-CSF (WAKO) and 10 ng/ml
352 IL-4 (WAKO) for 7 days. BMDCs were enriched by using CD11c MACS Beads
353 (Miltenyi Biotec) to remove dead cells generated during BMDC development.

354

355 **Cytokine production from tumor infiltrating lymphocytes**

Cells were isolated from tumors in mice 3 weeks after inoculation, and stimulated for 4 h with 50 ng/ml PMA and 500 ng/ml ionomycin. Brefeldin A (Sigma-Aldrich) was added for the last 3 h of culture. Cells were treated by using Foxp3 staining kits (eBioscience) and then stained with anti-IFN-γ mAb.

Immunohistochemistry and immunocytochemical staining

Paraffin-embedded tumor samples were deparaffinized in xylene and a series of graded concentrations of alcohol. To block endogenous horseradish peroxidase (HRP), tissue sections were incubated in 0.3% hydrogen peroxidase in methanol for 30 min at room temperature. For antigen retrieval, the specimens were preheated in AR6 buffer (PerkinElmer). Samples were incubated with anti-GFP (D5.1) XP (Cell signaling) or Rat anti-Foxp3 (FJK-16s; Thermo Fisher) for 1 h at room temperature or overnight at 4 °C, respectively and then incubated with appropriate secondary HRP-conjugated Abs. An HRP-conjugated dextran polymer system (PerkinElmer) was used for detection. After being washed with TBST, sections were mounted with 4',6-diamidino-2-phenylindole (DAPI; Vector labs). For quantification of Foxp3+ cells

372 in tumor tissues, tissue sections were scanned using BZ-X710 (Keyence). The number
373 of Foxp3+ cells per high-power field in each area was automatically counted with
374 hybrid cell counts software (Keyence). For immunocytochemical staining, 1.0×10^5
375 BMDCs were cultured in eight-well chamber slides (Thermo Fisher) and were
376 stimulated with pHrodo Red ester or pHrodo STP Green (Thermo Fisher)-labeled
377 exosomes. Cells were then fixed with 10% paraformaldehyde at 4 °C for 20 min,
378 permeabilized with 0.3% Triton-X, and then stained with rat a mAb to EEA-1 (1G11;
379 eBioscience) or TLR3 (11F8 ; Biolegend), followed by Alexa Flor 488-conjugated
380 donkey anti-mouse IgG or Alexa Flor 546-conjugated goat anti-rat IgG (Invitrogen),
381 respectively. Samples were evaluated by use of laser-scanning confocal microscopy
382 (FV10i FLOUVIEW; Olympus).
383
384 **In vivo depletion of Treg cells**
385 For in vivo depletion of Treg cells, mice were injected intraperitoneally with 300 μg of
386 an anti-CD25 mAb (PC61) and an isotype control Ab on days -6, -3, and 0 before B16
387 tumor inoculation.

388

389 **EV inhibitor treatment**

390 To inhibit EV generation, mice were injected with 1.0 mg/kg GW4869 (Ikebuchi et al.,

391 2018; Kosaka et al., 2013) (Cayman Chemical) intratumorally on days 14, 18, and 21

392 after tumor inoculation. Tumor tissues were harvested on day 25.

393

394 **Isolation and treatment of EVs**

395 B16 melanoma cells were cultured in complete RPMI supplemented with or without 2%

396 bovine serum albumin. The culture medium was harvested and subjected to sequential

397 centrifugation steps (first, 5 min for 2000G; second, 20 min for 10000G). EVs were

398 purified by using an Exosome Isolation Kit (WAKO) according to the manufacturer's

399 protocol. In brief, streptavidin magnetic beads, bound with biotinylated mouse Tim4-Fc,

400 which is the phosphatidylserine receptors, were added to the culture medium of B16

401 melanoma containing 2 mM $CaCl_2$, and the mixture was rotated for 3 h or overnight at

402 4 °C. The beads were washed three times with washing buffer and exosomes were

403 eluted with elution buffer (Fig. S3**A** and **B**). For quantification of the EVs in the elution

buffer, the concentration of EV protein was quantified by using a BCA Protein Assay Kit (Novagen). For BMDC stimulation by EVs, 2×10^5 BMDCs were incubated in the presence of 3 to 5 μg/ml EVs for 2.5 h. To inhibit TLR3 and TLR4 signaling, a TLR3/dsRNA complex inhibitor (Merck) and a TLR4 inhibitor (TAK-242; Merck) were added to the cultures of BMDCs for 15 min before exosome stimulation.

Coculture of iTreg cells with EV-stimulated BMDCs

CD4+ T cells were enriched from the spleen cells by using mouse CD4 MACS Beads (L3T4, Miltenyi Biotec) and then $CD4^+CD44^{lo}CD62L^{high}$Foxp3-eGFP$^-$ naïve T cells were purified by sorting with flow cytometry (FACS Aria III, Becton Dickinson). Inducible Treg cells were generated by culture of naïve $CD4^+$ T cells in the presence of plate-coated 0.33 μg/ml anti-CD3 Ab (145-2C11; TONBO), 2.0 μg/ml soluble CD28 (37.51; Biolegend), 20 ng/ml IL-2 (BD Pharmingen), and 2.5 ng/ml TGF-β (R&D system) for 3 days. Inducible Treg cells (5×10^4 cells/well) were cultured with exosome-stimulated BMDCs (5×10^4 cells/well) in 96-well round-bottom plates in the presence of IL-2 and TGF-β for 5 days.

Quantitative real-time PCR analysis

Total RNA was extracted from tumor-infiltrating CD11c+ cells and BMDCs. Reverse transcription was performed with a High-Capacity cDNA Reverse Transcription Kit (Applied Biosystems). Quantitative PCR analysis was performed with Power SYBER Green PCR Master Mix (Applied Biosystem) by using an ABI 7500 sequence detector (Applied Biosystems). The PCR primers are as follows: *Ifnb* fwd, 5′-cagctccaagaaaggacgaac-3′; *Ifnb* rev, 5′-ggcagtgtaactcttctgcat-3′; *Il10* fwd, 5′-gctggacaacatactgctaacc-3′; *Il10* rev, 5′- atttccgataaggcttggcaa-3′; and *Tgfb* fwd, 5′-tgacgtcactggagttgtacgg-3′; *Tgfb* rev, 5′-ggttcatgtcatggatggtgc-3′; normalization of quantitative real-time PCR was performed based on the gene encoding β-actin.

Western blots

BMDCs were stimulated or unstimulated with exosomes for 20 or 40 min and lysed with 1% NP-40. The lysetes of BMDCs were immunoblotted with antibody to phosphorylated IRF3 (4D4G; Cell Signaling Technology) or IRF3 (FL-425; Santa Cruz

436 Biotechnology).

437

438 **Bioinformatics**

439 For analysis of melanoma single cell RNA sequence (scRNA-seq), data were
440 downloaded from the database of scRNA-seq analysis of melanoma (accession no.:
441 GSE72056). The matrix data were passed to the R software package Seurat. Cells that
442 had unique gene counts of less than 200 were excluded, as were all genes that
443 were expressed in > 3 cells. Counted data were log2-transformed and scaled by
444 Seurat's *Scale Data* function. Principal component (PC) analysis was performed on a
445 set of highly variable genes defined by Seurat's *FindVariableGenes* function. Genes
446 associated the resulting PCs were then used for dimensionality reduction by using
447 t-distributed stochastic neighbor embedding (tSNE). Cluster-based marker identification
448 and differential expression were performed using Seurat's *FindAllmarkers*. RNA-seq
449 and survival data were obtained from The Cancer Genome Atlas (TCGA) project and
450 analyzed by using OncoLnc and GEPIA (Anaya, 2016; Tang et al., 2017).

451

452 **Statistical analyses**

453 Comparisons were performed using GraphPad Prism version 5.0 (GraphPad Software)
454 by one-way or two-way ANOVA, followed by Bonferroni's multiple comparisons test
455 or Student's unpaired t-test. Data are presented as means ± SEMs, and differences are
456 considered significant at $P<0.05$.

457

458 **Acknowledgments**

459 We thank Hisako Furugen, Satoko Tochihara and Wakako Saito for secretarial
460 assistance. This research was supported in part by grants provided by the Ministry of
461 Education, Culture, Sports, Science, and Technology of Japan (grant numbers 18H05022
462 and 16H06387 to A.S. and 19H03776 and 16H05350 to C.N-O.) and a grant-in-aid from
463 the Japan Society for the Promotion of Science Fellows (grant number 17J06167 to Y.N.).

464

465 **Competing interests**

466 The authors declare no competing financial interests.

467

468 **References**

469

470

471 Adeegbe DO, Nishikawa H. 2013. Natural and Induced T Regulatory Cells in
472 Cancer. *Frontiers in Immunology* **4**:190. doi:10.3389/fimmu.2013.00190
473 Anaya J. 2016. OncoLnc: linking TCGA survival data to mRNAs, miRNAs, and
474 lncRNAs. *PeerJ Computer Science* **2**:e67. doi:10.7717/peerj-cs.67
475 Andreola G, Rivoltini L, Castelli C, Huber V, Perego P, Deho P, Squarcina P,
476 Accornero P, Lozupone F, Lugini L, Stringaro A, Molinari A, Arancia G,
477 Gentile M, Parmiani G, Fais S. 2002. Induction of lymphocyte apoptosis by
478 tumor cell secretion of FasL-bearing microvesicles. *The Journal of*
479 *experimental medicine* **195**:1303–16. doi:10.1084/jem.20011624
480 Bedoui S, Whitney PG, Waithman J, Eidsmo L, Wakim L, Caminschi I, Allan RS,
481 Wojtasiak M, Shortman K, Carbone FR, Brooks AG, Heath WR. 2009.
482 Cross-presentation of viral and self antigens by skin-derived CD103+
483 dendritic cells. *Nature Immunology* **10**:488–495. doi:10.1038/ni.1724
484 Borrego F. 2013. The CD300 molecules: an emerging family of regulators of the
485 immune system. *Blood* **121**:1951–60. doi:10.1182/blood-2012-09-435057
486 Chen G, Huang AC, Zhang W, Zhang G, Wu M, Xu W, Yu Z, Yang J, Wang B,
487 Sun H, Xia H, Man Q, Zhong W, Antelo LF, Wu B, Xiong X, Liu X, Guan L, Li
488 T, Liu S, Yang R, Lu Youtao, Dong L, McGettigan S, Somasundaram R,
489 Radhakrishnan R, Mills G, Lu Yiling, Kim J, Chen YH, Dong H, Zhao Y,
490 Karakousis GC, Mitchell TC, Schuchter LM, Herlyn M, Wherry EJ, Xu X,
491 Guo W. 2018. Exosomal PD-L1 contributes to immunosuppression and is
492 associated with anti-PD-1 response. *Nature* **560**:382–386.
493 doi:10.1038/s41586-018-0392-8
494 Cheng K, Wang X, Yin H. 2011. Small-molecule inhibitors of the TLR3/dsRNA
495 complex. *Journal of the American Chemical Society* **133**:3764–7.
496 doi:10.1021/ja111312h
497 Clark G, Cooper B, Fitzpatrick S, Green B, Hart D. 2001. The gene encoding the
498 immunoregulatory signaling molecule CMRF-35A localized to human

chromosome 17 in close proximity to other members of the CMRF-35 family. *Tissue antigens* **57**:415–23. doi:10.1034/j.1399-0039.2001.057005415.x

Clayton A, Mitchell JP, Court J, Mason MD, Tabi Z. 2007. Human tumor-derived exosomes selectively impair lymphocyte responses to interleukin-2. *Cancer research* **67**:7458–66. doi:10.1158/0008-5472.CAN-06-3456

Couto N, Caja S, Maia J, Moraes MC, Costa-Silva B. 2018. Exosomes as emerging players in cancer biology. *Biochimie* **155**:2–10. doi:10.1016/j.biochi.2018.03.006

Francisco LM, Salinas VH, Brown KE, Vanguri VK, Freeman GJ, Kuchroo VK, Sharpe AH. 2009. PD-L1 regulates the development, maintenance, and function of induced regulatory T cells. *The Journal of Experimental Medicine* **206**:3015–3029. doi:10.1084/jem.20090847

Gangaplara A, Martens C, Dahlstrom E, Metidji A, Gokhale AS, Glass DD, Lopez-Ocasio M, Baur R, Kanakabandi K, Porcella SF, Shevach EM. 2018. Type I interferon signaling attenuates regulatory T cell function in viral infection and in the tumor microenvironment. *PLoS pathogens* **14**:e1006985. doi:10.1371/journal.ppat.1006985

Gao Y, Nish SA, Jiang R, Hou L, Licona-Limón P, Weinstein JS, Zhao H, Medzhitov R. 2013. Control of T Helper 2 Responses by Transcription Factor IRF4-Dependent Dendritic Cells. *Immunity* **39**:722–732. doi:10.1016/j.immuni.2013.08.028

Grange C, Tapparo M, Collino F, Vitillo L, Damasco C, Deregibus MC, Tetta C, Bussolati B, Camussi G. 2011. Microvesicles released from human renal cancer stem cells stimulate angiogenesis and formation of lung premetastatic niche. *Cancer research* **71**:5346–56. doi:10.1158/0008-5472.CAN-11-0241

Hsu P, Santner-Nanan B, Hu M, Skarratt K, Lee C, Stormon M, Wong M, Fuller SJ, Nanan R. 2015. IL-10 Potentiates Differentiation of Human Induced Regulatory T Cells via STAT3 and Foxo1. *The Journal of Immunology* **195**:3665–3674. doi:10.4049/jimmunol.1402898

Ikebuchi Y, Aoki S, Honma M, Hayashi M, Sugamori Y, Khan M, Kariya Y, Kato G, Tabata Y, Penninger JM, Udagawa N, Aoki K, Suzuki H. 2018. Coupling of

531 bone resorption and formation by RANKL reverse signalling. *Nature*
532 **561**:195–200. doi:10.1038/s41586-018-0482-7
533 Kim JM, Rasmussen JP, Rudensky AY. 2007. Regulatory T cells prevent
534 catastrophic autoimmunity throughout the lifespan of mice. *Nature*
535 *Immunology* **8**:191–197. doi:10.1038/ni1428
536 Klages K, Mayer CT, Lahl K, Loddenkemper C, Teng MWL, Ngiow SF, Smyth
537 MJ, Hamann A, Huehn J, Sparwasser T. 2010. Selective Depletion of Foxp3+
538 Regulatory T Cells Improves Effective Therapeutic Vaccination against
539 Established Melanoma. *Cancer Research* **70**:7788–7799.
540 doi:10.1158/0008-5472.CAN-10-1736
541 Kosaka N, Iguchi H, Hagiwara K, Yoshioka Y, Takeshita F, Ochiya T. 2013.
542 Neutral sphingomyelinase 2 (nSMase2)-dependent exosomal transfer of
543 angiogenic microRNAs regulate cancer cell metastasis. *The Journal of*
544 *biological chemistry* **288**:10849–59. doi:10.1074/jbc.M112.446831
545 Kosaka N, Iguchi H, Yoshioka Y, Takeshita F, Matsuki Y, Ochiya T. 2010.
546 Secretory Mechanisms and Intercellular Transfer of MicroRNAs in Living
547 Cells. *Journal of Biological Chemistry* **285**:17442–17452.
548 doi:10.1074/jbc.M110.107821
549 Lima LG, Chammas R, Monteiro RQ, Moreira MC, Barcinski MA. 2009.
550 Tumor-derived microvesicles modulate the establishment of metastatic
551 melanoma in a phosphatidylserine-dependent manner. *Cancer Letters* 168–
552 175. doi:10.1016/j.canlet.2009.03.041
553 Liu Y, Gu Y, Han Y, Zhang Q, Jiang Z, Zhang X, Huang B, Xu X, Zheng J, Cao X.
554 2016. Tumor Exosomal RNAs Promote Lung Pre-metastatic Niche Formation
555 by Activating Alveolar Epithelial TLR3 to Recruit Neutrophils. *Cancer cell*
556 **30**:243–56. doi:10.1016/j.ccell.2016.06.021
557 Medrano RF, Hunger A, Mendonça SA, Barbuto JM, Strauss BE. 2017.
558 Immunomodulatory and antitumor effects of type I interferons and their
559 application in cancer therapy. *Oncotarget* **8**:71249–71284.
560 doi:10.18632/oncotarget.19531
561 Melo SA, Luecke LB, Kahlert C, Fernandez AF, Gammon ST, Kaye J, LeBleu VS,
562 Mittendorf EA, Weitz J, Rahbari N, Reissfelder C, Pilarsky C, Fraga MF,

563 Piwnica-Worms D, Kalluri R. 2015. Glypican-1 identifies cancer exosomes
564 and detects early pancreatic cancer. *Nature* **523**:177.
565 doi:10.1038/nature14581
566 Metidji A, Rieder SA, Glass DD, Cremer I, Punkosdy GA, Shevach EM. 2015.
567 IFN-α/β receptor signaling promotes regulatory T cell development and
568 function under stress conditions. *Journal of immunology (Baltimore, Md :*
569 *1950)* **194**:4265–76. doi:10.4049/jimmunol.1500036
570 Minn AJ. 2015. Interferons and the Immunogenic Effects of Cancer Therapy.
571 *Trends in Immunology* **36**:725–737. doi:10.1016/j.it.2015.09.007
572 Morimoto Y, Kishida T, Kotani S, Takayama K, Mazda O. 2018. Interferon-β
573 signal may up-regulate PD-L1 expression through IRF9-dependent and
574 independent pathways in lung cancer cells. *Biochemical and Biophysical*
575 *Research Communications* **507**:330–336. doi:10.1016/j.bbrc.2018.11.035
576 Mougiakakos D, Johansson CC, Trocme E, All-Ericsson C, Economou MA,
577 Larsson O, Seregard S, Kiessling R. 2010. Intratumoral forkhead box
578 P3-positive regulatory T cells predict poor survival in
579 cyclooxygenase-2-positive uveal melanoma. *Cancer* **116**:2224–33.
580 doi:10.1002/cncr.24999
581 Muller L, Simms P, Hong C-S, Nishimura MI, Jackson EK, Watkins SC,
582 Whiteside TL. 2017. Human tumor-derived exosomes (TEX) regulate Treg
583 functions via cell surface signaling rather than uptake mechanisms.
584 *OncoImmunology* **6**:e1261243. doi:10.1080/2162402X.2016.1261243
585 Nakahashi-Oda C, Tahara-Hanaoka S, Honda S, Shibuya K, Shibuya A. 2012a.
586 Identification of phosphatidylserine as a ligand for the CD300a
587 immunoreceptor. *Biochemical and biophysical research communications*
588 **417**:646–50. doi:10.1016/j.bbrc.2011.12.025
589 Nakahashi-Oda C, Tahara-Hanaoka S, Shoji M, Okoshi Y, Nakano-Yokomizo T,
590 Ohkohchi N, Yasui T, Kikutani H, Honda S, Shibuya K, Nagata S, Shibuya A.
591 2012b. Apoptotic cells suppress mast cell inflammatory responses via the
592 CD300a immunoreceptor. *The Journal of experimental medicine* **209**:1493–
593 503. doi:10.1084/jem.20120096
594 Nakahashi-Oda C, Udayanga K, Nakamura Y, Nakazawa Y, Totsuka N, Miki H,

595 Iino S, Tahara-Hanaoka S, Honda S, Shibuya K, Shibuya A. 2016. Apoptotic
596 epithelial cells control the abundance of Treg cells at barrier surfaces. *Nature*
597 *Immunology* **17**:441–450. doi:10.1038/ni.3345
598 Niel VG, D'Angelo G, cell RG reviews. 2018. Shedding light on the cell biology
599 of extracellular vesicles. doi:10.1038/nrm.2017.125
600 Nishikawa H, Sakaguchi S. 2010. Regulatory T cells in tumor immunity.
601 *International Journal of Cancer* **127**:759–767. doi:10.1002/ijc.25429
602 Ondondo B, Jones E, Godkin A, Gallimore A. 2013. Home sweet home: the
603 tumor microenvironment as a haven for regulatory T cells. *Frontiers in*
604 *immunology* **4**:197. doi:10.3389/fimmu.2013.00197
605 Onizuka S, Tawara I, Shimizu J, Sakaguchi S, Fujita T, Nakayama E. 1999.
606 Tumor rejection by in vivo administration of anti-CD25 (interleukin-2
607 receptor alpha) monoclonal antibody. *Cancer research* **59**:3128–33.
608 Patidar A, Selvaraj S, Sarode A, Chauhan P, Chattopadhyay D, Saha B. 2018.
609 DAMP-TLR-cytokine axis dictates the fate of tumor. *Cytokine* **104**:114–123.
610 doi:10.1016/j.cyto.2017.10.004
611 Ramsdell F, Ziegler SF. 2014. FOXP3 and scurfy: how it all began. *Nature*
612 *reviews Immunology* **14**:343–9. doi:10.1038/nri3650
613 Sarkar SN, Peters KL, Elco CP, Sakamoto S, Pal S, Sen GC. 2004. Novel roles of
614 TLR3 tyrosine phosphorylation and PI3 kinase in double-stranded RNA
615 signaling. *Nature structural & molecular biology* **11**:1060–7.
616 doi:10.1038/nsmb847
617 Sawant DV, Yano H, Chikina M, Zhang Q, Liao M, Liu C, Callahan DJ, Sun Z,
618 Sun T, Tabib T, Pennathur A, Corry DB, Luketich JD, Lafyatis R, Chen W,
619 Poholek AC, Bruno TC, Workman CJ, Vignali DAA. 2019. Adaptive plasticity
620 of IL-10+ and IL-35+ Treg cells cooperatively promotes tumor T cell
621 exhaustion. *Nature Immunology* **20**:724–735.
622 doi:10.1038/s41590-019-0346-9
623 Shitara K, Nishikawa H. 2018. Regulatory T cells: a potential target in cancer
624 immunotherapy. *Annals of the New York Academy of Sciences* **1417**:104–115.
625 doi:10.1111/nyas.13625
626 Skog J, Würdinger T, Rijn S van, Meijer DH, Gainche L, Sena-Esteves M, Curry

627 WT, Carter BS, Krichevsky AM, Breakefield XO. 2008. Glioblastoma
628 microvesicles transport RNA and proteins that promote tumour growth and
629 provide diagnostic biomarkers. *Nature cell biology* **10**:1470–6.
630 doi:10.1038/ncb1800
631 Srivastava S, Koch MA, Pepper M, Campbell DJ. 2014. Type I interferons
632 directly inhibit regulatory T cells to allow optimal antiviral T cell responses
633 during acute LCMV infection. *The Journal of experimental medicine*
634 **211**:961–74. doi:10.1084/jem.20131556
635 Szajnik M, Czystowska M, Szczepanski MJ, Mandapathil M, Whiteside TL. 2010.
636 Tumor-derived microvesicles induce, expand and up-regulate biological
637 activities of human regulatory T cells (Treg). *PloS one* **5**:e11469.
638 doi:10.1371/journal.pone.0011469
639 Tang Z, Li Chenwei, Kang B, Gao G, Li Cheng, Zhang Z. 2017. GEPIA: a web
640 server for cancer and normal gene expression profiling and interactive
641 analyses. *Nucleic acids research* **45**:W98–W102. doi:10.1093/nar/gkx247
642 Tatematsu M, Nishikawa F, Seya T, Matsumoto M. 2013. Toll-like receptor 3
643 recognizes incomplete stem structures in single-stranded viral RNA. *Nature*
644 *communications* **4**:1833. doi:10.1038/ncomms2857
645 Voss OH, Tian L, Murakami Y, Coligan JE, Krzewski K. 2015. Emerging role of
646 CD300 receptors in regulating myeloid cell efferocytosis. *Molecular & cellular*
647 *oncology* **2**:e964625. doi:10.4161/23723548.2014.964625
648 Wan YY, Flavell RA. 2007. 'Yin–Yang' functions of transforming growth factor-
649 β and T regulatory cells in immune regulation. *Immunological Reviews*
650 **220**:199–213. doi:10.1111/j.1600-065X.2007.00565.x
651 Wang X, Luo G, Zhang K, Cao J, Huang C, Jiang T, Liu B, Su L, Qiu Z. 2018.
652 Hypoxic Tumor-Derived Exosomal miR-301a Mediates M2 Macrophage
653 Polarization via PTEN/PI3Kγ to Promote Pancreatic Cancer Metastasis.
654 *Cancer research* **78**:4586–4598. doi:10.1158/0008-5472.CAN-17-3841
655 Wang Y, Nakahashi-Oda C, Okayama Y, Shibuya A. 2019. Autonomous
656 regulation of IgE-mediated mast cell degranulation and immediate
657 hypersensitivity reaction by an inhibitory receptor CD300a. *The Journal of*
658 *allergy and clinical immunology* **144**:323-327.e7.

659 doi:10.1016/j.jaci.2019.03.005
660 Wieckowski EU, Visus C, Szajnik M, Szczepanski MJ, Storkus WJ, Whiteside TL.
661 2009. Tumor-Derived Microvesicles Promote Regulatory T Cell Expansion
662 and Induce Apoptosis in Tumor-Reactive Activated CD8+ T Lymphocytes.
663 *The Journal of Immunology* **183**:3720–3730. doi:10.4049/jimmunol.0900970
664 Witwer KW, Théry C. 2019. Extracellular vesicles or exosomes? On primacy,
665 precision, and popularity influencing a choice of nomenclature. *J Extracell*
666 *Vesicles* **8**:1648167. doi:10.1080/20013078.2019.1648167
667 Xiao W, Klement JD, Lu C, Ibrahim ML, Liu K. 2018. IFNAR1 Controls
668 Autocrine Type I IFN Regulation of PD-L1 Expression in Myeloid-Derived
669 Suppressor Cells. *Journal of immunology (Baltimore, Md : 1950)* **201**:264–277.
670 doi:10.4049/jimmunol.1800129
671 Ying X, Wu Q, Wu X, Zhu Q, Wang Xinjing, Jiang L, Chen X, Wang Xipeng.
672 2016. Epithelial ovarian cancer-secreted exosomal miR-222-3p induces
673 polarization of tumor-associated macrophages. *Oncotarget* **7**:43076–43087.
674 doi:10.18632/oncotarget.9246
675 Yotsumoto K, Okoshi Y, Shibuya K, Yamazaki S, Tahara-Hanaoka S, Honda S-I,
676 Osawa M, Kuroiwa A, Matsuda Y, Tenen DG, Iwama A, Nakauchi H, Shibuya
677 A. 2003. Paired activating and inhibitory immunoglobulin-like receptors,
678 MAIR-I and MAIR-II, regulate mast cell and macrophage activation. *The*
679 *Journal of experimental medicine* **198**:223–33. doi:10.1084/jem.20021825
680 Zitvogel L, Galluzzi L, Kepp O, Smyth MJ, Kroemer G. 2015. Type I interferons
681 in anticancer immunity. *Nature Reviews Immunology* **15**:405–414.
682 doi:10.1038/nri3845

683